

Title: Feasibility of Extracting Tissues Material Properties via Cohesive Elements: A Finite Element Approach to Probe Insertion Procedures in non-Invasive Spine Surgeries

First Author: Ibrahim El Bojairami

Second Author: Amirhossein Hamedzadeh

Corresponding Author: Mark Driscoll, P.Eng., Ph.D*

Authors Affiliations: Musculoskeletal Biomechanics Research Lab, Department of Mechanical Engineering, McGill University, Montréal, Quebec, Canada

Corresponding Author Address: Department of Mechanical Engineering, Musculoskeletal Biomechanics Research Laboratory, McGill University, 817 Sherbrooke Street West, Montreal, QC, H3A 0C3, Macdonald Eng. Bldg. Office #153, Canada

Corresponding Author Telephone: +1-514-398-6299

Corresponding Author Fax Number: +1-514-398-7365

Corresponding Author E-mail Address: mark.driscoll@mcgill.ca

Corresponding Author ORCID iD: <https://orcid.org/0000-0002-5348-6054>

First Author ORCID iD: <https://orcid.org/0000-0002-2463-0897>

Manuscript Word Count: 6546

Abstract Word Count: 292

Number of Figures: 9

Number of Tables: 2

ABSTRACT

Introduction: Modelling the mechanical behavior of soft tissues probe insertion remains a challenging endeavor due to involved interdependent phenomena comprising tissues nonlinear deformation, contact between the probe and the tissue, crack propagation, and viscoelastic effects. To that matter, cohesive elements allow simulating crack formation and propagation, which provides a promising path to modelling the mechanical behavior of probe insertion in soft tissues. *Objective:* As such, the aim of the present study was to investigate the feasibility of devising and integrating an algorithm in a finite element (FE) case-study in efforts of reverse-engineering the material properties of non-homogeneous soft tissues. *Methodology:* A layered nonlinear tissue model with a cohesive zone was created in the commercial software ABAQUS. Material properties were iteratively modified via a hybrid gradient descent optimization algorithm: Minimizing the resultant error to firstly find optimum Ogden's hyperelastic parameters, followed by obtaining the damage parameters. Perceived material properties were then compared to those obtained via experimental human cadaver testing. *Results:* Under the investigated four-layered muscles model, numerical results overlapped, to a great extent, with six different force-insertion experimental profiles with an average error of $\pm 15\%$. The best profile fit was realized when the highest sudden force drop was less than 60% of the peak force. Lastly, the FE analysis revealed an increase in stiffness as the probe advanced inside the tissue. *Conclusions:* The optimization algorithm demonstrated its capability to reverse engineer the material parameters required for the FE analysis of real, non-homogeneous, soft tissues. The significance of this procedure lies within its ability to extract tissues material parameters, in real-time, with little to no intervention or invasive experimental tests. This could potentially further serve as a database for different muscle layers and force-insertion profiles, used for surgeons and physicians clinical training purposes.

KEY WORDS

Finite element analysis, probe insertion, cohesive elements, tissues material properties, optimization algorithms.

INTRODUCTION

Needle insertion is a common practice in numerous medical procedures such as endoscopy [1], spine biopsy [2], and epidural lumbar puncture [3]. Traditionally, physicians and surgeons are trained on these procedures via either cadavers or anesthetized animals [4]. Considering the associated challenges, such as patient's safety and limited exposure to cadaveric samples [4], the use of virtual reality (VR) as a comprehensive training tool has gained momentum [5]. However, simulating an accurate VR environment, in terms of probe insertion, is a must to realize a precise surgical simulator tool [6].

Numerous approaches have been realized to model probe insertions, with most studies focusing on robotically controlled needle insertion and steering flexible needles in the tissue [7], [8]. Other studies were concerned with obtaining the elastic and fracture properties of the tissue [9]. Generally, the insertion force f_p is subdivided into three components, namely, friction $f_{friction}$, force required to cut the tissue $f_{cutting}$, and reaction force resulting from tissue deformation $f_{stiffness}$ [10], as follows:

$$f_p(\mathcal{Y}) = f_{friction}(\mathcal{Y}) + f_{cutting}(\mathcal{Y}) + f_{stiffness}(\mathcal{Y}) \quad (1)$$

A more convenient approach is to express the same concept in terms of energies [11], [12] such that:

$$W_{ext} = \widehat{W}_f + \widehat{W}_E + \widehat{W}_{cr} \quad (2)$$

where W_{ext} is the external work, \widehat{W}_f is the frictional work, \widehat{W}_E is the strain energy, and \widehat{W}_{cr} is the work required for crack propagation. Among these components, the strain energy is the only recoverable term, which makes it a primary candidate for Finite Element (FE) modelling as energy frameworks are well-suited for FE applications.

Although FE analyses are computationally expensive in nature, their real-time application is still attractive when combined with condensation techniques [13]. In this particular case, a planar-based tissue was modelled, whereby boundary and local material conditions changes were achieved via low-rank matrix updates. Furthermore, the needle was modelled as a beam, comprising one-dimensional elements. This added advantage was appropriate as beam elements accommodate for large-strain deformations.

In essence, the problem of probe insertion is mechanical based, with different levels of complexity and assumptions [14]. Broadly speaking, several phenomena simultaneously happen in a quasi-static probe insertion problem, mainly tissue elastic deformation, propagation of the crack in the tissue, and hard normal and tangential contact between the probe and the tissue [15]–[17]. The interdependency between these phenomena further adds to the problem's complexity. For instance, the contact surface between the tissue and the probe is directly related to the crack propagation. That is, as the probe cuts through the tissue, frictional forces increase as the contact surface expands; however, if the crack propagates ahead of the probe tip, the tissue relaxes and the contact will be lost between the tissue and the probe [17].

Crack propagation is perhaps the most complex phenomenon to model due to both, the theoretical and computational aspects of the problem [18]. A well-known approach in fracture mechanics is the J-integral method, originally applied to metal plasticity [19]. In this approach, rupture is considered as a sudden crack propagation when the release rate of the strain potential surpasses the fracture toughness

of the material. Under dynamic conditions where tissue viscoelastic effects are of interest, the J-integral is combined with a nonlinear Kelvin-Voigt model [20].

Another widely used approach to fracture mechanics is the use of cohesive elements, whereby the tearing is described by the surface separation of the cohesive interface [21], [22]. In cohesive theories, the separation between the two surfaces is described as a displacement jump, resisted by the cohesive traction, ahead of the crack tip [23]. The expediency of this approach has pushed researchers to exploit it in several applications including modelling aorta dissection [24] via utilizing both, the extended and classical FE methods [23]. It has been also used to investigate the effect of bevel-tip steerable needles [25], whereby a cohesive zone at the tip of the needle was adopted to simulate elements separation. The primary finding was that the forces at the tip of the needle were highly sensitive to the tissue's fracture toughness. Lastly, cohesive elements were utilized in dynamic explicit methods to simulate needle insertions [26]. The strain energy release during the crack formation was extracted from experimental data, to which the FE model was calibrated based on the needle insertion in a homogeneous phantom tissue experimental set [26]. The needle was further assumed a rigid body and a single layer of cohesive elements were placed between the tissue elements to model the crack path. Fundamentally, the study concluded the accuracy of cohesive approaches to capture gross aspects of needle insertion operations [26].

In light of the aforementioned studies, to date, and to the best of the authors' knowledge, needle insertion FE simulations focus on controlled phantom experiments [25], [26], with little to no knowledge on the feasibility of their application in real-time surgeries under unknown material properties. This in no means is to say that much advancement has not been made in the fields of modelling surgeries, biological tissues fracture, needle insertions, and tool-tissue interactions. There has rather been an exponential progress in such fields amid the emergence of powerful simulation techniques and computational power. A comprehensive review of needle insertion into soft tissues with a focus on the force measurements effect to model the interaction between needles and tissues

can be found in [15]. Within this, several FE models were developed, ranging from tissues deformation during needle insertion in soft tissue [13], [27], [28], 2D FE modeling of needle insertion with application to prostate brachytherapy [29], [30], to force feedback models relevant to epidural insertion [31]–[33]. Real-time simulations of tool-tissues interactions have also experienced significant improvements thanks to GPU-based implementations [34]. One critical accompanied limitation is the solution accuracy, which has been fully addressed in a recent application of corotational cut finite element method to needle insertion simulations by combining an error control method with an adaptive meshing technique [35], [36]. However, retaining patient-specific material properties whilst the surgery is in effect remains a dilemma.

The purpose of the current work is to devise an algorithm, coupled with a FE probe insertion simulation, to reverse-engineer the material properties of a non-homogeneous tissue during intervertebral disc (IVD) discectomy. The study follows a recent experimental work [37], which was further used as the comparable, to investigate the feasibility of gaining access to tissues' material behavior during surgery. Although the current numerical approach follows the work of Oldfield et al. [26], it differs from previous contributions as it adopts a hybrid gradient-descent algorithm to create different muscle layers with different material properties in order to fit reaction forces from the FE simulation to the experimental data set.

METHODOLOGY

Cohesive Elements Description

To better understand the mode of operation of cohesive elements, their constitutive response in terms of traction-separation laws is first briefly covered. In 2D problems, the nominal traction stress vector for cohesive elements has two components, t_n and t_s , representing the normal and shear tractions along the local 1-direction and the local 2-direction, respectively. The corresponding separations are

denoted δ_n and δ_s . Denoting by T_0 the original thickness of the cohesive element, the nominal strains are then defined as:

$$\varepsilon_n = \frac{\delta_n}{T_0}, \varepsilon_s = \frac{\delta_s}{T_0} \quad (3)$$

The elastic behavior is then described by:

$$\mathbf{t} = \begin{Bmatrix} t_n \\ t_s \end{Bmatrix} = \begin{bmatrix} E_{nn} & E_{ns} \\ E_{sn} & E_{ss} \end{bmatrix} \begin{Bmatrix} \varepsilon_n \\ \varepsilon_s \end{Bmatrix} = \mathbf{E}\boldsymbol{\varepsilon} \quad (4)$$

where E is the elastic modulus, with E_{nn} and E_{ss} being the normal and tangential elastic moduli components. In this study, uncoupled cohesive traction behavior is desired, to which the off-diagonal components, E_{ns} and E_{sn} , are zero. The element thickness is chosen to be 1 ($T_0 = 1$).

Figure 1 demonstrates the linear separation-traction law for a typical cohesive element. The damage initiates at $\delta_{n,s}^0$ and progresses to the full extent when the displacement reaches $\delta'_{n,s}$. G_c is the fracture toughness denoted and is equal to the shaded area. Damage is assumed to initiate when the maximum nominal stress ratio, defined by the expression below, reaches a value of 1. Denoting σ_{mn} and σ_{ms} to be the peak values of the nominal stress when the deformation is either purely normal to the interface or purely in the shear direction, respectively, the criterion is represented as:

$$\text{Max} \left\{ \frac{\langle t_n \rangle}{\sigma_{mn}}, \frac{t_s}{\sigma_{ms}} \right\} = 1 \quad (5)$$

where $\langle \dots \rangle$ is the Macaulay brackets operator. At this point, the element loses all strength and is removed from the analysis.

Finite Element Model

An axisymmetric FE model comprising the four major muscle layers encountered in lumbar IVD discectomy, namely the latissimus dorsi, iliocostalis, longissimus, and multifidus, was created in ABAQUS, Dassault Systèmes. The model closely followed the experimental procedures conducted by

El-Monajjed and Driscoll [37] for validation and comparison purposes. A replica of a standard surgical probe tool used in spinal fusion surgeries, mimicking a ball pen dilator, was modelled (Figure 2-c). The tool conceived a 0.5 mm rounded tip, with a minor and major diameter of 1 and 4 mm, respectively, over a 7 mm length. The original tool material was medical grade stainless steel 304, which was treated as a discrete rigid body in the FE model to mimic the almost null-deformation behavior during surgeries [38]. Muscle layers were separated via a thin fascial layer to mimic lumbar muscles anatomy (Figure 2-a and 2-b). To retain the inherent nonlinear, hyperelastic, nature of human muscles, each muscle layer was modelled via an incompressible Ogden material behavior [39], due to its high level of accuracy in capturing the nonlinear steep change in soft tissues force-deformation curve [40]:

$$U(\mathbf{F}(X, t)) = \frac{2\mu}{\alpha^2} (\lambda_1^\alpha + \lambda_2^\alpha + \lambda_3^\alpha - 3) + \frac{1}{D} (J - 1)^2 \quad (6)$$

where U is the strain potential, \mathbf{F} is the deformation gradient, λ_i are the principal stretches characterized by the eigenvalues of deformation, and J represents muscle's bulk modulus.

As previously mentioned, skeletal muscles are inherently incompressible, thus, to mimic this behavior and simplify the model to a new-Hookean, the J and α parameters, which qualitatively represent muscle's bulk modulus and fractional exponent, were set to 1 and 2, respectively [41]–[43]. As such, the material behavior collapses to the following 1-degree, optimization-compatible, function that follows a behavior similar to the neo-Hookean:

$$U(\mathbf{F}(X, t)) = \frac{\mu}{2} (\lambda_1^2 + \lambda_2^2 + \lambda_3^2 - 3) \quad (7)$$

Modelling fracture within the cohesive zone requires careful choice of the model parameters. That is, unless one of the damage parameters of Figure 1, namely σ_{mn} , \mathbf{G}_c , or K , is predefined, the resultant scheme would be ill-defined. Besides, to perform a realistic simulation of the cutting process, δ_n^0 and δ_n' need to be fundamentally constrained to the geometry of the indenter [14]. As such, δ_n' was

constrained to be less than the 4 mm maximum diameter of the needle while δ_n^0 was assumed to be less than or equal to its 1 mm minor diameter. If these conditions are not fulfilled, a complete cut would not be achieved. All other parameters were left without bounds. On the other hand, σ_{mn} and G_c should be obtained from dedicated experiments; however, this is a challenging task due to the large strains preceding failure, dependence on strain rates, and failure stress variabilities between different muscle layers. To this matter, with the aid of conducted experiments [37], an estimate of the elastic opening of the crack, K , could be obtained. However, a bad choice of K could introduce an additional fictitious compliance to the bulk material, to which previous investigators have suggested keeping this value as high as possible [44], [45]. As such, for the purpose of this study being a feasibility assessment of tissue material properties, rather than picking a random value, a maximum derivative finder was coded in Python and iterated over the experimental force-displacement curves [37] to obtain the highest possible initial stiffness as a best estimate of K , which resulted with $K = 11.2 \text{ MPa/mm}$, a relatively high value compared to soft tissue elastic response. All other parameters were randomly assigned a positive starting point.

In line with the previously conducted experimental study [37], the modelled muscle layers had 25 mm radius, whereas a 50 mm depth subdivided over four torso muscles as follows: Latissimus dorsi starts at 0 and ends at 16 mm, Iliocostalis starts at 17 and ends at 22 mm, Longissimus starts at 23 and ends at 30 mm, and Multifidus extends from 31 mm to the very ends, with a 1mm fascial layer between every other muscle. A 2 mm deep notch was created at the contact point between the tissue and the probe. The model was meshed via linear quadrilateral elements (CAX4R), with the exception of the crack path being meshed with cohesive linear quadrilateral elements (COHAX4), both in the XZ plane (Figure 2-b). Encastre boundary conditions were applied to the bottom of the tissue, while a frictional contact, of 0.3 friction coefficient derived from bone-muscle interaction [46], was maintained between the tool and tissue, especially at the cohesive zone. This has the advantage of preventing the tool from penetrating tissue elements. That is, the tool pushes on the current cohesive

element until the damage criterion is met. The cohesive element is then removed from the simulation and the tool progresses to the next element. Given the time-independent nonlinear quasi-static nature of the problem, an iterative implicit solver was used.

In line with the experimental setup [37], the probe can only move along the y-axis. The experiments were designed to mimic the mechanical interaction of a multi-purpose probe to access the intervertebral disc (IVD) for a general postero-lateral, minimally invasive, spinal lumbar interbody fusion surgery. The probe punctures through the four different torso muscle layers, in a series of six different puncture tests, in efforts of gaining access to the first three lumbar IVDs (IVDs of L1-L2, L2-L3, and L3-L4), from both the left and right side.

Optimization Scheme

As previously stated, the goal of this study was to investigate the feasibility of obtaining material properties and force profiles of a probe insertion in different torso muscle layers via an optimization algorithm. The adopted algorithm is the gradient descent method (GDM) [47], a well-known optimization method vastly used in machine learning. Since the investigated study is a 2D small-scale axisymmetric problem, the use of GDM would be highly advantageous due to the method's simplicity and fast computational power per iteration [48]. Python (Python Software Foundation) was utilized to run the algorithm, whereby at each step, material behavior values were returned to ABAQUS to run the numerical case-scenario.

The error function used in this study was defined as follows:

$$\varepsilon(X, Y) = \theta_j (X_j - Y_j)^2 \tag{8}$$

$$\theta_j = 1 \tag{9}$$

where θ_j s are the expression weights, whereas X_j and Y_j are the reaction forces from the FE analysis and the experimental case-studies, respectively. The error thus becomes a function of the muscle layers material properties and the damage parameters of the cohesive zone illustrated in Figure 1. Therefore, the variation of the error function can be expressed as:

$$\delta\varepsilon(\boldsymbol{\mu}, \mathbf{D}) = \frac{\delta\varepsilon}{\delta\boldsymbol{\mu}} \delta\boldsymbol{\mu} + \frac{\delta\varepsilon}{\delta\mathbf{D}} \delta\mathbf{D} \quad (10)$$

$$\boldsymbol{\mu} = (\mu_1, \mu_2, \dots, \mu_i) \quad (11)$$

$$\mathbf{D} = (K_1, \sigma_{1mn}, \mathbf{G}_{1c}, \delta_{n,1}^0, \delta'_{n,1}, \dots, K_i, \sigma_{imn}, \mathbf{G}_{ic}, \delta_{n,i}^0, \delta'_{n,i}) \quad (12)$$

where μ_i , ($i \in \mathbb{N}$), is the shear modulus of the i -th muscle layer while K_i , σ_{imn} , \mathbf{G}_{ic} , $\delta_{n,i}^0$, and $\delta'_{n,i}$ ($i \in \mathbb{N}$), are the crack opening stiffness, maximum nominal stress, fracture toughness, crack initiation displacement, and critical failure displacement of the i -th cohesive layer, respectively. As previously stated, the purpose of the cohesive elements is to initiate a crack and allows for the probe to follow an incision path. As such, a homogeneous material property for the bulk modelled tissue is of interest. To fulfill this, the algorithm minimizes the error function with respect to $\boldsymbol{\mu}$ of the muscle layers, restricted to positive moduli only, assuming a high 11.2 MPa/mm initial crack opening stiffness, with a 10% allowance constraint during optimization, to prevent any added compliance to the bulk material, as well as constraining δ_n^0 to be less than or equal to needle's 1 mm minor diameter as part of geometry constraints. The set of μ_i , K_i , and δ_n^0 that minimize μ_i 's error function are returned (Figure 3, line 16) to form a new error function ($\hat{\varepsilon}$, Figure 3, line 18), to which the weights θ_j s are then increased in value for points with critical drops. These points are identified via computing the derivative of the force-displacement profile of the experimental results. The new error function $\hat{\varepsilon}$ is then minimized with respect to the remaining critical cohesive parameters (\mathbf{D}), as explained in Figure 3, to find the optimum σ_{mn} , \mathbf{G}_{ic} , and δ'_n values, under the 4 mm geometric constraints set for δ'_n .

Experimental Case-Studies

The experimental tests [37] were conducted to mimic and characterize the mechanical interaction of a multi-purpose probe at the initial stage to achieve access to IVDs during minimally invasive, lumbar spine, interbody fusion surgery. During the surgery, the probe is manually handled by surgeons to penetrate through multiple muscle layers, mainly back spine muscles. Prior to insertion, a 10-15 mm deep incision is placed at the point of access through the skin and Thoracolumbar Fascia (TLF). The experimental test protocols are devised to investigate probe insertion, relaxation, and extraction. The tests were conducted on a custom-made hydraulic traction/compression machine (MTS 858 BIONIX II, MTS Systems Corporation, USA). It is equipped with a 100 N axial load test with a resolution of 0.02 N. The probe was inserted at a constant 0.5 mm/s axial speed. The overall penetration cut-off was set to 40 mm displacement and 70 N axial force. One trial was performed per vertebral level (L1-L2, L2-L3, and L3-L4) per side (left/Right). The cadaver was situated at an angle on the MTS machine frame at which the probe insertion was directly perpendicular to the tissue.

RESULTS

Ogden material properties parameter results, for the muscle layers under study, are shown in Table 1. The latissimus dorsi of L1-L2-L showed similar modulus, μ , to that of L1-L2-R, whereas the iliocostalis muscle of L1-L2-L was significantly stronger (73%). The same was true for the longissimus muscle, being even stiffer than the iliocostalis. Multifidus was of particular interest, conveying relatively small μ values, as compared to the other muscle layers. On the other hand, the first step optimization constraints of δ_n^0 and K , as well as the optimization of the second error function allowed for obtaining average cohesive material properties for each of the six puncture tests (Table 2). Fracture toughness ranged between 0.99 and 5.34 KJ/m² whereas maximum nominal stress was

between 0.71 and 3.71 MPa for all puncture points. The corresponding crack opening stiffness, crack initiation displacement, and critical failure displacements are also reported in Table 2.

In addition, Figures 4 through 9 illustrate both, the FE and the experimental forces obtained from the six puncture tests on the different muscle layers. The FE results were better at predicting the first significant drop, explained by the probe transitioning from the latissimus dorsi to the iliocostalis muscle. The force acquired by the FE L3-L4-R puncture test had the best agreement with the experimental results. Furthermore, although the first drop was significant for the L1-L2-L case (6 N), the FE simulation was still able to successfully predict it; however, it overestimated the maximum force by 16%. Similarly, for the second and third drops, as the probe penetrated the longissimus and multifidus muscles, respectively, FE results were in good agreement with the experimental curves, recording an average error ranging between 11 and 17%.

DISCUSSION

The overarching goal of this study was to devise a FE method and an optimization algorithm to investigate the feasibility of obtaining the material properties of muscles, along replicating the experimental results, obtained from probe insertion during a general minimally invasive, lumbar spine, interbody fusion surgery. To the best of the authors' knowledge, most attempts on finite element simulation of needle insertion are focused on controlled experiments on phantom [25], [26]. However, in real time analysis or during surgery, it is not viable to conduct experimental tests to obtain the material properties, required for FE simulation. Moreover, the complexity of tissue composition makes it arduous to obtain the underlying descriptive material behavior. This is due to the fact that material properties along the depth of the tissue, or across its width, can potentially drastically vary. In addition, although not perfectly bonded together, muscle layers are still encompassed by fascia and connective tissues, which in turn induce variations on muscles' material

behavior. In fact, numerous studies have shown that fascia and connective tissues possess significantly higher stiffness than adjacent muscles [49]–[53]. In general, they are stronger and can undergo significantly high deformations (300%). In this study, thin layers of fascia (1 mm) were placed in between the muscle layers in order to investigate their effect on the overall insertion profile (Figure 2). It was expected that fascia layers would have a significant effect due to their much stiffer material properties. In contrast, only local spikes were observed in the insertion force profiles (Figures 4 through 9), which was explained by the fact that actual fascia models were replaced by thin layers to maintain the focus on muscles. So to speak, if fascia and connective tissues were properly modelled, as illustrated by previous research conducted by the current authors [49], their realistic role might have appeared. However, since the focus was merely on muscles material properties, it was decided to replace them with simpler models to ease the FE simulations.

Even though this was the case, this still caused random numerical instabilities, explained by the elements distorting excessively under small loads, which can be attributed to finite sliding contact algorithm. Generally speaking, this issue results whenever adjacent objects are not in perfect bonded contact state. For the current study, a frictional contact was placed to mimic the behavior of a tool pushing on the tissue of interest. Although accompanied with numerical instabilities in some cases, this is still highly advantageous to prevent the tool from penetrating elements that has not met the damage criterion yet. Nevertheless, such numerical instabilities were overcome by appropriately refining the mesh at the contact points. In addition, such refinements resulted with a highly compatible mesh, with global and local mesh quality exceeding 95%. This being the case, and considering that the study was a feasibility analysis, a mesh sensitivity analysis was not necessary anymore given the accuracy of the original mesh.

Force profiles (Figures 4 through 9) showed the potential feasibility of the underlined methods to predict the material properties of soft tissues via FE techniques to a relatively high accuracy level. However, differences were still observed between the experimental and numerical results, reflected by

the average errors reported in Table 1. In-vivo tissue biomechanics experiments are usually affected by numerous factors including age, gender, and genetics. The experimental tests were conducted on the same cadaver, under the same physiological condition, thus minimizing such experimental errors. On the other hand, observed errors were mainly due to simplifications realized in the FE model, mainly performing the analysis under static conditions. Other minor simplifications were assuming a rigid tool, choosing an initial stiffness starting point, and fixing some of Ogden's constitutive model parameters based on the theory and literature. However, such simplifications were reasonable and complied with literature, and although they led to marginal errors, they made the feasibility and convergence of the FE model and the optimization scheme possible.

Constraints and assumptions made regarding the cohesive zone model might have also affected material properties results. The necessity for predefining at least one damage parameter for the optimization to work drastically affected the results. Defining an initial crack opening stiffness that is both realistic and sufficiently high to avoid introducing added compliance to the material was highly challenging. Although every effort was made to extract this K value from experimental values, slight changes in this parameter might render completely different cohesive parameters, to which the authors recommend performing dedicated experiments to obtain such parameter prior to running the optimization scheme in real-time. On the other hand, although fluctuations were observed with respect to reported fracture toughness, such results were in the vicinity of similar literature experiments [9], [54]. Lastly, crack initiation and failure displacements were within needle geometric constraints, showing a realistic crack propagation and cutting mechanism.

This study offered a feasible solution to bridge the gap between the mechanical behavior of the tissue and its material properties by utilizing an algorithm to reverse engineer properties required for FE simulations. However, conceived material properties do not necessarily reflect the values that are obtained from other mechanical tests. This is due to the complicated mechanical nature of soft tissues, as well as limitations involved not only in experimental works, but also in the theoretical realm of

damage and fracture mechanics. Nevertheless, cohesive parameters (Equation 12), especially fracture toughness, is a nonlocal variable, meaning that it is affected by the extent of damage at its vicinity. That is, approaches of determining fracture toughness based on single numerical elements might render inaccurate results, whereby fracture from adjacent elements affect local results. Thus, the need for more sophisticated models, such as the phase-field method, which not only consider local, but also gradient variations [55]. Nonetheless, besides being computationally expensive, such models are incompatible with current available FE commercial software, making their real-time implementation questionable.

Limitations

Similar to any in silico model, limitations are always present due to the FE approximation and GDM optimization schemes. However, with assumptions kept to a minimum, this does not limit method's capabilities in assessing the feasibility of collecting real-time biomechanical behavior of tissues. For the method to converge, it assumes a static behavior, which is a valid assumption as the experiments were passively performed on isolated muscles, thus eliminating their active contraction part [56]. A thorough study was also previously conducted by the current authors on utilizing static material properties to approximate tissues realistic behavior [49]. Furthermore, as explained in the methodology, muscles are inherently incompressible, thus suggesting the values used for Ogden's J and α parameters. Although it would be ideal to also optimize these material parameters, realistic values were chosen in order for the GDM algorithm to quickly converge. Another limitation was the use of the GDM scheme instead of other faster and more accurate methods such as control gradient and fast gradient descent algorithms. However, considering that GDM does not compute any second derivatives, making it inherently computationally fast per iteration, this was a reasonable choice due to model's simplicity and scale [48]. Besides, its practical use is well-developed in literature, as well as being backed by most current available commercial FE software. One last major limitation was the

need for a manual initial K starting point for the algorithm to proceed. However, this did not pose any problems for the current research as this value was extrapolated from the conducted experimental case-studies. On the other hand, although this study developed a successful approach to obtain feasible tissue material properties, extensive validation and comparison against other parameters outside the presented modelling approach is still required. This is particularly important in order to investigate whether all fracture and tissue mechanisms were accurately incorporated and modelled. Thus, dedicated validation might still be essential before using the reported parameters outside the enclosed modelling problem. Nevertheless, such simplifications are potentially valid and do not hinder the method's capabilities to obtain feasible tissue material behavior.

Future Work

The FE-based algorithm presented in this study was capable of reverse engineering feasible parameters to model probe insertion in non-homogenous tissues. Even though the initial guess was manually tuned, the rest of the procedure was performed with little intervention. With such a promising algorithm, in future research, the authors aim to fully automate and enhance the scheme via resolving some of its major limitations, in order to implement it for surgeons training applications. As such, the method would become compatible with more detailed FE simulations, allowing to extract more advanced information, such as real-time stress distributions and muscles pressure. Another goal is to cross-examine the method's results against in-vivo experimental tests to find meaningful correlations, empirical formulas, and build material databases for the design of patient-specific probes.

CONCLUSIONS

This study investigated the feasibility of utilizing the cohesive element approach in the simulation of probe insertion in non homogenous cadaveric tissues. The study offered a gradient descent method-based algorithm to obtain feasible set of material parameters for different torso muscles. To achieve the best fit, the algorithm minimized a predefined error function with equal weights to obtain Ogden's μ shear modulus parameters of each muscle layer. The weights were then adjusted to the critical experimental drop point, intensifying their effect on the new error function, to which a second stage new error function was minimized in order to find the cohesive zone material parameters. Numerical simulation results presented good agreement with conducted experiments, showing an average difference of 15% attributed to FE limitations and simplifications necessary for the optimization to have worked. This method is potentially promising and can be used to generate realistic force-insertion curves, within the statistical variance of experimental results, for virtual surgery training applications.

ACKNOWLEDGMENT

We gratefully acknowledge funding by McGill University (MEDA), the Fonds de Recherche du Québec – Nature et Technologies (FRQNT), and the Natural Sciences and Engineering Research Center (NSERC).

CONFLICT OF INTEREST

To the best of our knowledge, this research has no conflict of interest for any of the authors.

REFERENCES

- [1] T. Itoi *et al.*, "Experimental endoscopy: objective evaluation of EUS needles," *Gastrointest. Endosc.*, 2009.

- [2] W. C. G. Peh, "CT-guided percutaneous biopsy of spinal lesions," *Biomedical Imaging and Intervention Journal*. 2006.
- [3] C. M. Doherty and R. B. Forbes, "Diagnostic lumbar puncture," *Ulster Med. J.*, 2014.
- [4] D. Stefanidis, T. C. Yonce, J. M. Green, and A. P. Coker, "Cadavers versus pigs: Which are better for procedural training of surgery residents outside the OR?," *Surg. (United States)*, 2013.
- [5] R. McCloy and R. Stone, "Virtual reality in surgery," *BMJ*, 2001.
- [6] K. S. Gurusamy, R. Aggarwal, L. Palanivelu, and B. R. Davidson, "Virtual reality training for surgical trainees in laparoscopic surgery," *Cochrane Database of Systematic Reviews*. 2009.
- [7] H. Delingette, "Toward realistic soft-tissue modeling in medical simulation," *Proc. IEEE*, 1998.
- [8] S. Y. Ko, B. L. Davies, and F. Rodriguez Y Baena, "Two-dimensional needle steering with a 'programmable bevel' inspired by nature: Modeling preliminaries," in *IEEE/RSJ 2010 International Conference on Intelligent Robots and Systems, IROS 2010 - Conference Proceedings*, 2010.
- [9] T. Azar and V. Hayward, "Estimation of the fracture toughness of soft tissue from needle insertion," in *Lecture Notes in Computer Science (including subseries Lecture Notes in Artificial Intelligence and Lecture Notes in Bioinformatics)*, 2008.
- [10] A. M. Okamura, C. Simone, and M. D. O'Leary, "Force modeling for needle insertion into soft tissue," *IEEE Trans. Biomed. Eng.*, 2004.
- [11] C. Simone and A. M. Okamura, "Modeling of needle insertion forces for robot-assisted percutaneous therapy," in *Proceedings - IEEE International Conference on Robotics and*

Automation, 2002.

- [12] S. Misra, K. B. Reed, B. W. Schafer, K. T. Ramesh, and A. M. Okamura, "Mechanics of flexible needles robotically steered through soft tissue," *Int. J. Rob. Res.*, 2010.
- [13] S. P. Dimaio and S. E. Salcudean, "Needle steering and motion planning in soft tissues," *IEEE Transactions on Biomedical Engineering*. 2005.
- [14] M. Terzano, D. Dini, F. Rodriguez y Baena, A. Spagnoli, and M. Oldfield, "An adaptive finite element model for steerable needles," *Biomech. Model. Mechanobiol.*, 2020.
- [15] N. Abolhassani, R. Patel, and M. Moallem, "Needle insertion into soft tissue: A survey," *Med. Eng. Phys.*, 2007.
- [16] D. J. van Gerwen, J. Dankelman, and J. J. van den Dobbelsteen, "Needle-tissue interaction forces - A survey of experimental data," *Medical Engineering and Physics*. 2012.
- [17] R. Taschereau, J. Pouliot, J. Roy, and D. Tremblay, "Seed misplacement and stabilizing needles in transperineal permanent prostate implants," *Radiother. Oncol.*, 2000.
- [18] X. Su, Z. Yang, and G. Liu, "Finite element modelling of complex 3D static and dynamic crack propagation by embedding cohesive elements in Abaqus," *Acta Mech. Solida Sin.*, 2010.
- [19] J. R. Rice, "Inelastic constitutive relations for solids: An internal-variable theory and its application to metal plasticity," *J. Mech. Phys. Solids*, 1971.
- [20] M. Mahvash and P. E. Dupont, "Mechanics of dynamic needle insertion into a biological material," *IEEE Trans. Biomed. Eng.*, 2010.
- [21] M. Ortiz and A. Pandolfi, "Finite-deformation irreversible cohesive elements for three-dimensional crack-propagation analysis," *Int. J. Numer. Methods Eng.*, 1999.
- [22] K. K. Mathur, A. Needleman, and V. Tvergaard, "Three dimensional analysis of dynamic

- ductile crack growth in a thin plate,” *J. Mech. Phys. Solids*, 1996.
- [23] A. Ferrara and A. Pandolfi, “A numerical study of arterial media dissection processes,” in *International Journal of Fracture*, 2010.
- [24] T. C. Gasser and G. A. Holzapfel, “Geometrically non-linear and consistently linearized embedded strong discontinuity models for 3D problems with an application to the dissection analysis of soft biological tissues,” *Comput. Methods Appl. Mech. Eng.*, 2003.
- [25] S. Misra, K. B. Reed, A. S. Douglas, K. T. Ramesh, and A. M. Okamura, “Needle-tissue interaction forces for bevel-tip steerable needles,” in *Proceedings of the 2nd Biennial IEEE/RAS-EMBS International Conference on Biomedical Robotics and Biomechanics, BioRob 2008*, 2008.
- [26] M. Oldfield, D. Dini, G. Giordano, and F. Rodriguez y Baena, “Detailed finite element modelling of deep needle insertions into a soft tissue phantom using a cohesive approach,” *Comput. Methods Biomech. Biomed. Engin.*, 2013.
- [27] S. P. DiMaio and S. E. Salcudean, “Interactive simulation of needle insertion models,” *IEEE Trans. Biomed. Eng.*, 2005.
- [28] S. P. DiMaio and S. E. Salcudean, “Needle steering and model-based trajectory planning,” *Lect. Notes Comput. Sci. (including Subser. Lect. Notes Artif. Intell. Lect. Notes Bioinformatics)*, 2003.
- [29] R. Alterovitz, J. Pouliot, R. Taschereau, I. C. Joe Hsu, and K. Goldberg, “Simulating needle insertion and radioactive seed implantation for prostate brachytherapy,” in *Studies in Health Technology and Informatics*, 2003.
- [30] R. Alterovitz, K. Goldberg, J. Pouliot, R. Taschereau, and I. C. Hsu, “Needle insertion and radioactive seed implantation in human tissues: Simulation and sensitivity analysis,” in

Proceedings - IEEE International Conference on Robotics and Automation, 2003.

- [31] L. Hiemenz, D. Stredney, and P. Schmalbrock, "Development of the force-feedback model for an epidural needle insertion simulator," in *Studies in Health Technology and Informatics*, 1998.
- [32] L. L. H. Holton, "Force models for needle insertion created from measured needle puncture data," in *Studies in Health Technology and Informatics*, 2001.
- [33] B. H. MEIKLEJOHN, "The effect of rotation of an epidural needle: An in vitro study," *Anaesthesia*, 1987.
- [34] H. Courtecuisse, J. Allard, P. Kerfriden, S. P. A. Bordas, S. Cotin, and C. Duriez, "Real-time simulation of contact and cutting of heterogeneous soft-tissues," *Med. Image Anal.*, 2014.
- [35] H. P. Bui, S. Tomar, and S. P. A. Bordas, "Corotational cut finite element method for real-time surgical simulation: Application to needle insertion simulation," *Comput. Methods Appl. Mech. Eng.*, 2019.
- [36] H. P. Bui, S. Tomar, H. Courtecuisse, S. Cotin, and S. P. A. Bordas, "Real-Time Error Control for Surgical Simulation," *IEEE Trans. Biomed. Eng.*, 2018.
- [37] K. El-Monajjed and M. Driscoll, "Analysis of Surgical Forces Required to Gain Access Using a Probe for Minimally Invasive Spine Surgery via Cadaveric-Based Experiments towards Use in Training Simulators," *IEEE Trans. Biomed. Eng.*, 2021.
- [38] R. Craker, B. V. Johnson, H. Sakthivel, and D. J. Cappelleri, "Design of a miniaturized actuation system for robotic lumbar discectomy tools," in *Proceedings of the ASME Design Engineering Technical Conference*, 2020.
- [39] R. W. O. Fu, Y. B., "Nonlinear Elasticity: Theory and Applications," *Nonlinear Elast. Theory*

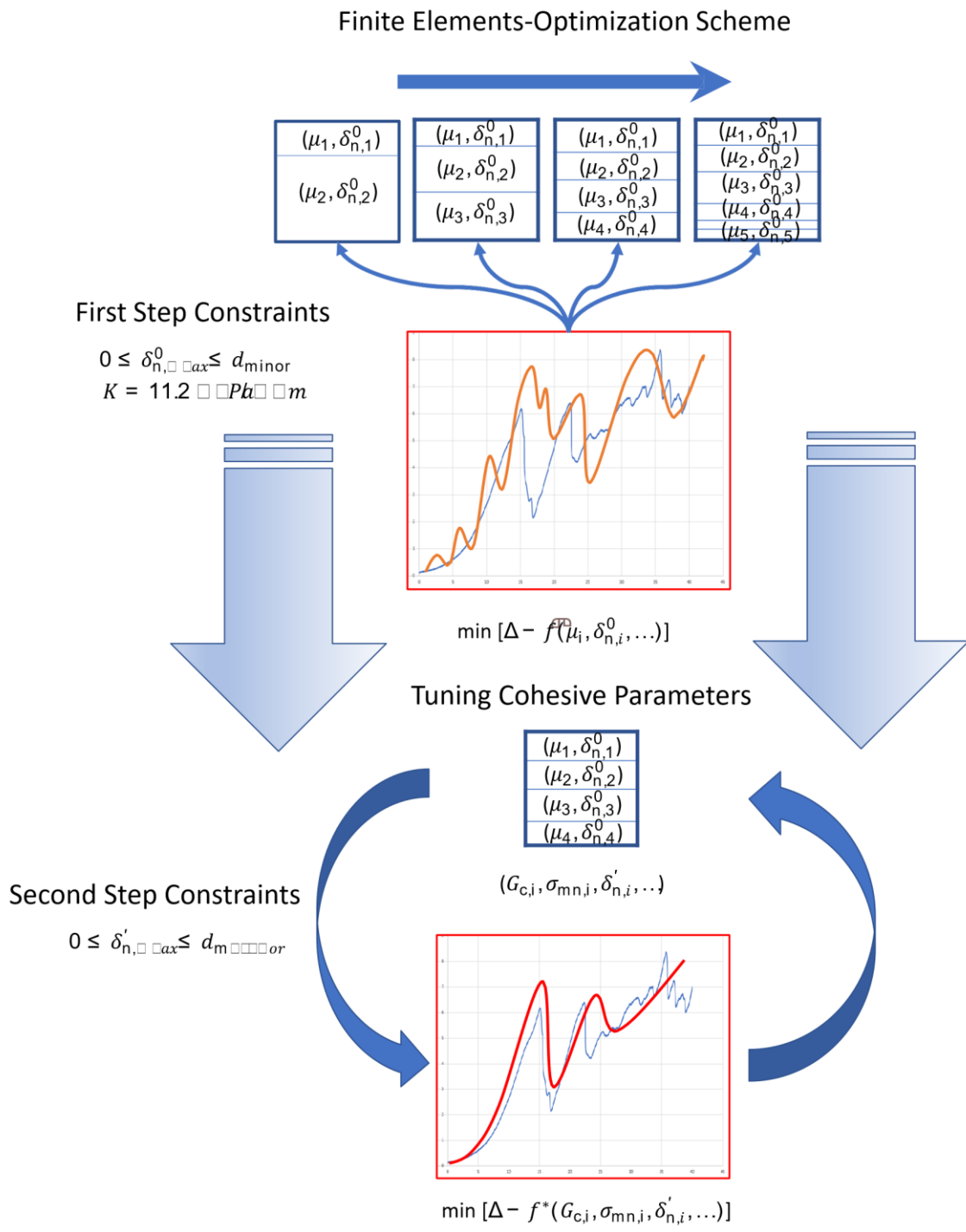
- Appl.*, 2001.
- [40] P. A. L. S. Martins, R. M. N. Jorge, and A. J. M. Ferreira, "A comparative study of several material models for prediction of hyperelastic properties: Application to silicone-rubber and soft tissues," *Strain*, 2006.
- [41] F. Mo, Z. Zheng, H. Zhang, G. Li, Z. Yang, and D. Sun, "In vitro compressive properties of skeletal muscles and inverse finite element analysis: Comparison of human versus animals," *J. Biomech.*, 2020.
- [42] N. Elyasi, K. K. Taheri, K. Narooei, and A. K. Taheri, "A study of hyperelastic models for predicting the mechanical behavior of extensor apparatus," *Biomech. Model. Mechanobiol.*, 2017.
- [43] N. Fougeron, P. Y. Rohan, D. Haering, J. L. Rose, X. Bonnet, and H. Pillet, "Combining Freehand Ultrasound-Based Indentation and Inverse Finite Element Modeling for the Identification of Hyperelastic Material Properties of Thigh Soft Tissues," *J. Biomech. Eng.*, 2020.
- [44] R. de Borst, "Numerical aspects of cohesive-zone models," *Eng. Fract. Mech.*, 2003.
- [45] I. Scheider, "Cohesive model for crack propagation analyses of structures with elastic – plastic material behavior," *GKSS Res. center, Geesthacht*, 2001.
- [46] S. Shacham, D. Castel, and A. Gefen, "Measurements of the static friction coefficient between bone and muscle tissues," *J. Biomech. Eng.*, 2010.
- [47] Z. Michalewicz, "Genetic Algorithms, Numerical Optimization, and Constraints," *Proc. sixth Int. Conf. Genet. algorithms*, 1995.
- [48] A. El Mouatasim, "Fast gradient descent algorithm for image classification with neural

networks," *Signal, Image Video Process.*, 2020.

- [49] I. El Bojairami, K. El-Monajjed, and M. Driscoll, "Development and validation of a timely and representative finite element human spine model for biomechanical simulations," *Sci. Rep.*, 2020.
- [50] C. M. Eng, F. Q. Pancheri, D. E. Lieberman, A. A. Biewener, and L. Dorfmann, "Directional differences in the biaxial material properties of fascia lata and the implications for fascia function," *Ann. Biomed. Eng.*, 2014.
- [51] L. H. Yahia, P. Pigeon, and E. A. DesRosiers, "Viscoelastic properties of the human lumbodorsal fascia," *J. Biomed. Eng.*, 1993.
- [52] C. D. Dora, D. S. Dimarco, M. E. Zobitz, and D. S. Elliott, "Time dependent variations in biomechanical properties of cadaveric fascia, porcine dermis, porcine small intestine submucosa, polypropylene mesh and autologous fascia in the rabbit model: Implications for sling surgery," *J. Urol.*, 2004.
- [53] R. Schleip, A. Zorn, and W. Klingler, "Biomechanical properties of fascial tissues and their role as pain generators," *J. Musculoskelet. Pain*, vol. 18, no. 4, pp. 393–395, 2010.
- [54] D. Taylor, N. O'Mara, E. Ryan, M. Takaza, and C. Simms, "The fracture toughness of soft tissues," *J. Mech. Behav. Biomed. Mater.*, 2012.
- [55] O. Gültekin and G. A. Holzapfel, "A brief review on computational modeling of rupture in soft biological tissues," in *Computational Methods in Applied Sciences*, 2018.
- [56] E. M. H. Bosboom, M. K. C. Hesselink, C. W. J. Oomens, C. V. C. Bouten, M. R. Drost, and F. P. T. Baaijens, "Passive transverse mechanical properties of skeletal muscle under in vivo compression," *J. Biomech.*, 2001.

This is a post-peer-review, pre-copyedit version of an article published in Medical and Biological Engineering and Computing . The final authenticated version is available online at: "10.1007/s11517-021-02432-9". The following terms of use apply:
<https://www.springer.com/gb/open-access/publication-policies/self-archiving-policy>

GRAPHICAL ABSTRACT



FIGURES

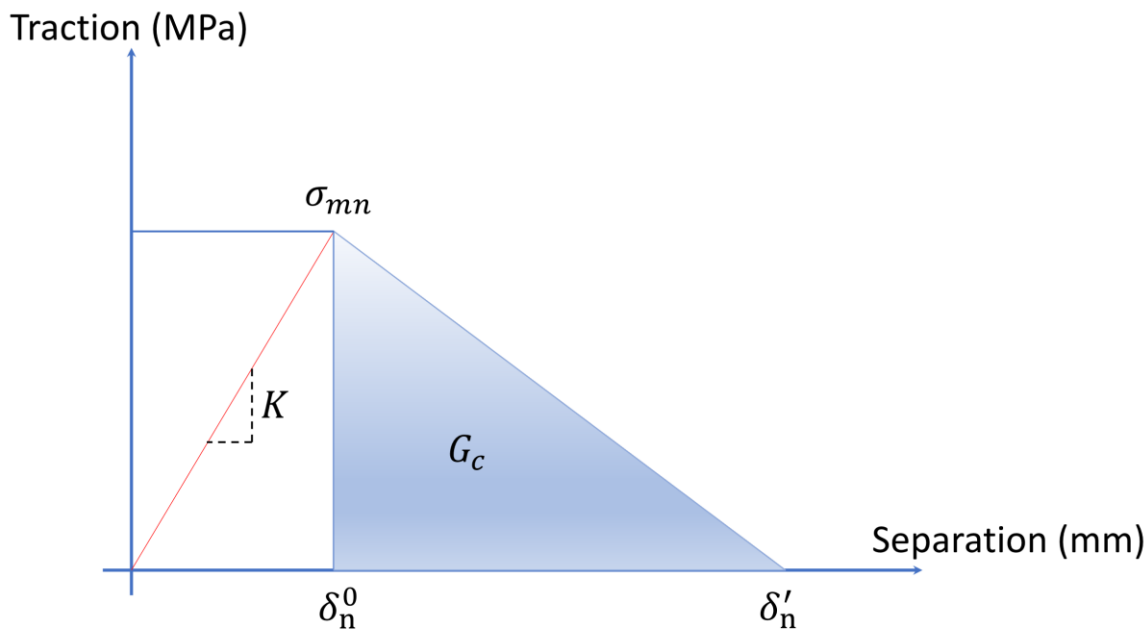


Fig. 1 Linear separation-traction behavior for cohesive elements

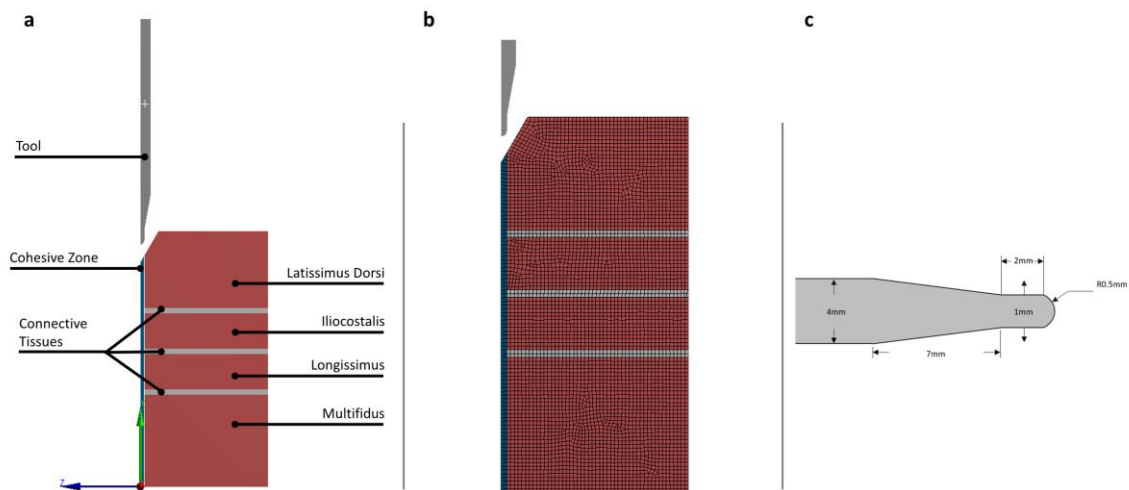


Fig. 2 (a) Probe-muscle layers FE model, (b) Adopted FE mesh, (c) schematic of the utilized probe

```

1: procedure MIN  $\varepsilon(\mu, \sigma_{mn}, G_c, \delta_n^0, \delta_n')$  ▷ Minimizing the error
2:   $\mu_0 \leftarrow (\mu_1, \mu_2, \dots); K^0 \leftarrow K_{\text{ax}}; \delta_{n, \text{ax}}^0 \leq d_{\text{ax}}; \delta_{n, \text{ax}}' \leq d_{m \text{ or}}$ 
3:   $\delta_n^0 \leftarrow (\delta_{n,1}^0, \delta_{n,2}^0, \dots)$ 
4:   $\delta_n' \leftarrow (\delta_{n,1}', \delta_{n,2}', \dots)$  ▷ Initializing  $\mu, K, \sigma_{mn}, G_c, \delta_n^0, \delta_n'$ 
5:   $\sigma_{mn}^0 \leftarrow (\sigma_{mn,1}, \sigma_{mn,2}, \dots)$ 
6:   $G_c^0 \leftarrow (G_{c,1}, G_{c,2}, \dots)$ 
7:   $N \leftarrow 0$  ▷ initiate counter  $N$ 
8:  while  $\varepsilon(\mu^{n+1}, K^{n+1}, \delta_{n+1}^0, \delta_n', \sigma_{mn}^0, G_c^0) \leq \varepsilon(\mu^n, K^n, \delta_n^0, \delta_n', \sigma_{mn}^0, G_c^0)$  &  $(\delta_{n, \text{ax}}^0 \leq d_{\text{ax}})$ , do
9:     $\beta^n \leftarrow \frac{(\mu^n - \mu^{n-1})^T [\varepsilon(\mu^n) - \varepsilon(\mu^{n-1})]}{\varepsilon(\mu^n) - \varepsilon(\mu^{n-1})}$  ▷ Gradient descent for  $\mu$ 
10:     $\mu^{n+1} \leftarrow \mu^n - \beta^n (\mu^n)$ 
11:     $\delta_{n+1}^0 \leftarrow \delta_n^0 - \beta^n (\delta_n^0)$ 
12:     $K^{n+1} \leftarrow K^n - \beta^n (K^n)$ 
13:     $N \leftarrow n + 1$  ▷ update the value of the counter
14:  end while
15:  Update  $\theta_j \leftarrow \hat{\theta}_j$  ▷ new weights for the new error function
16:  return  $\mu^*, \delta_n^{0*}, K^* \leftarrow \mu^N, \delta_n^0, K^N$  ▷ Optimized  $\mu, \delta_n^0$ , and  $K$  values
17:   $\varepsilon(\mu^0, K^0, \delta_n^0, \delta_n', \sigma_m^0, G^0)$ 
18:   $\varepsilon(D^0) \leftarrow \varepsilon(\mu^*, \delta_n^{0*}, K^*, \delta_n', \sigma_{mn}^0, G_c^0)$ 
19:  while  $\varepsilon(D^{n+1}) \leq \varepsilon(D^n)$  do
20:     $\beta^n \leftarrow \frac{(D^n - D^{n-1})^T [\nabla \varepsilon(D^n) - \nabla \varepsilon(D^{n-1})]}{\nabla \varepsilon(D^n) - \nabla \varepsilon(D^{n-1})}$ 
21:     $D^{n+1} \leftarrow D^n - \beta^n \nabla \varepsilon(D^n)$ 
22:  end while
23: end procedure

```

Fig. 3 Gradient Descent Method-based optimization and curve fitting algorithm for the finite element model

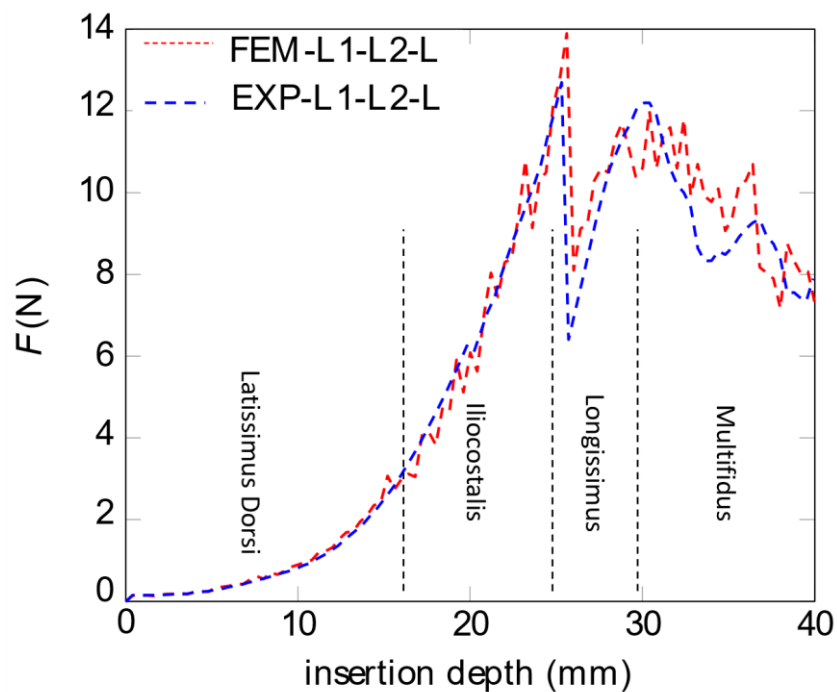


Fig. 4 Probe insertion force-depth profile for L1-L2-L puncture case

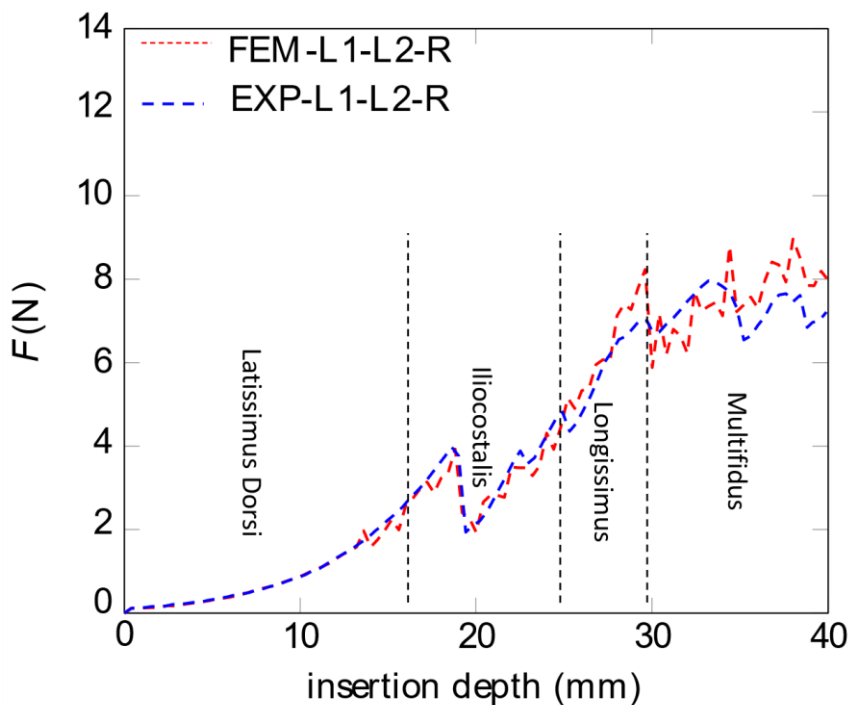


Fig. 5 Probe insertion force-depth profile for L1-L2-R puncture case

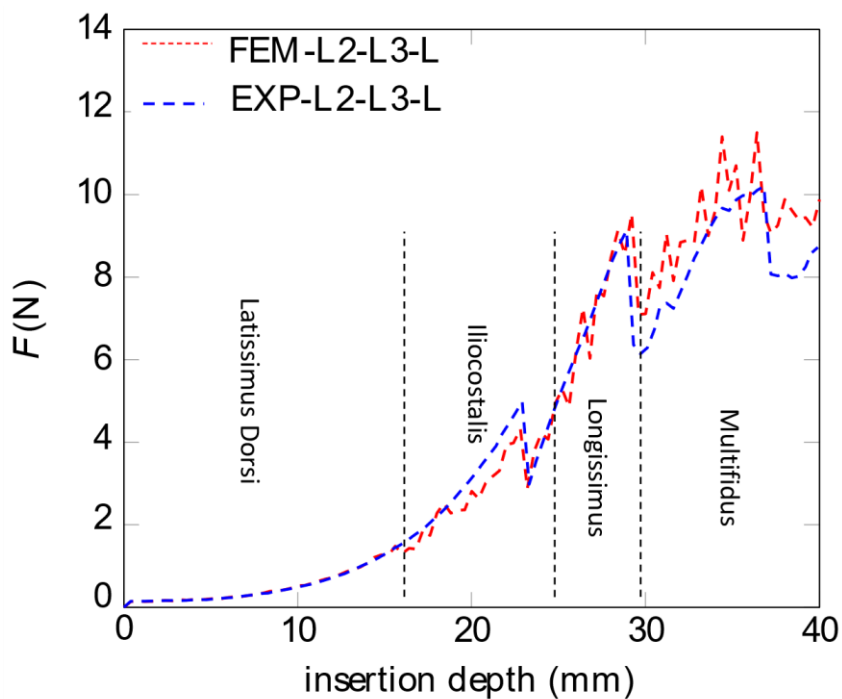


Fig. 6 Probe insertion force-depth profile for L2-L3-L puncture case

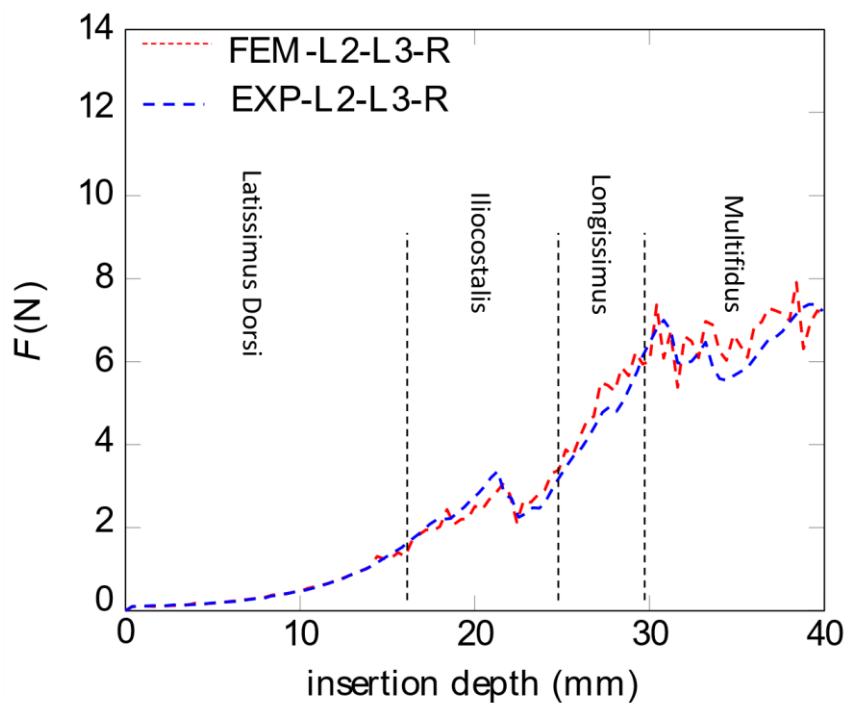


Fig. 7 Probe insertion force-depth profile for L2-L3-R puncture case

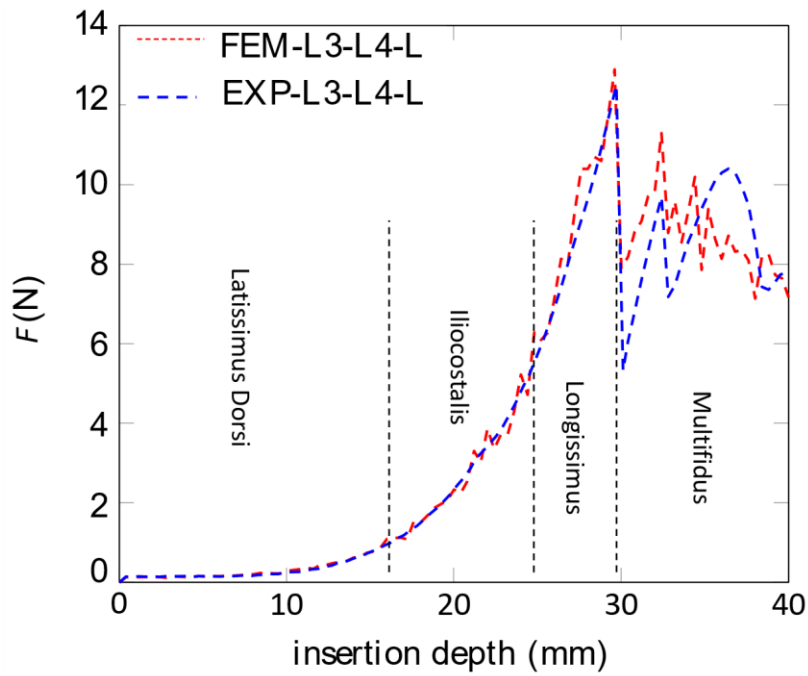


Fig. 8 Probe insertion force-depth profile for L3-L4-L puncture case

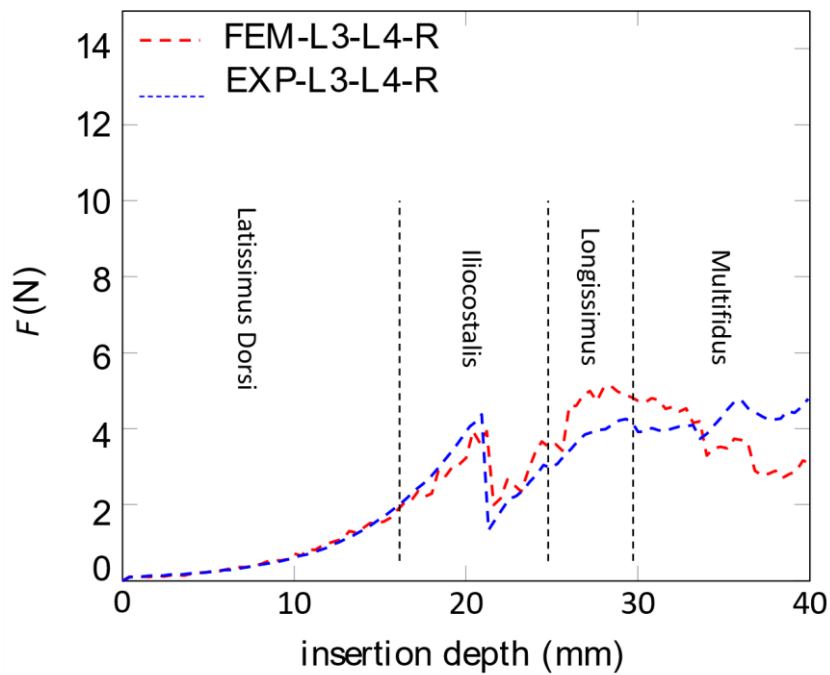


Fig. 9 Probe insertion force-depth profile for L3-L4-R puncture case

TABLES

Location	Muscle Hyperelasticity Parameter μ_i (KPa)				
	Latissimus Dorsi μ_1	Iliocostalis μ_2	Longissimus μ_3	Multifidus μ_4	Average Error (%)
L1-L2-L	9.3	45.3	52.3	0.1	12
L1-L2-R	9.3	26.0	26.5	7.6	14
L2-L3-L	6.7	43.0	42.6	8.4	12
L2-L3-R	6.7	30.0	31.0	12.8	11
L3-L4-L	4.3	45.0	50.0	0.16	13
L3-L4-R	7.0	8.0	8.5	0.08	17

Table 1: Ogden material parameters for the different muscle layers

Location	Maximum Nominal Stress σ_{mn} (MPa)	Fracture Toughness G_c (KJ/m ²)	Crack Opening Stiffness K (MPa/mm)	Crack Initiation Displacement δ_n^0 (mm)	Critical Failure Displacement δ_n' (mm)
L1-L2-L	2.3	2.71	11.1	0.21	2.36
L1-L2-R	1.34	0.99	10.3	0.13	1.49
L2-L3-L	1.58	1.35	10.5	0.15	1.71
L2-L3-R	0.71	0.42	10.1	0.07	1.2
L3-L4-L	3.71	5.34	10.3	0.36	2.88
L3-L4-R	2.62	4.45	10.9	0.24	3.4

Table 2: Cohesive zone parameters